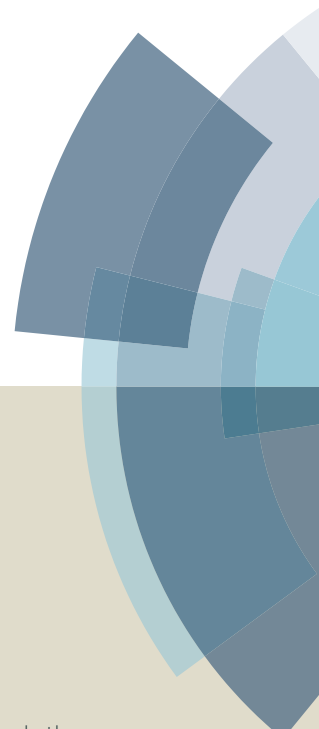
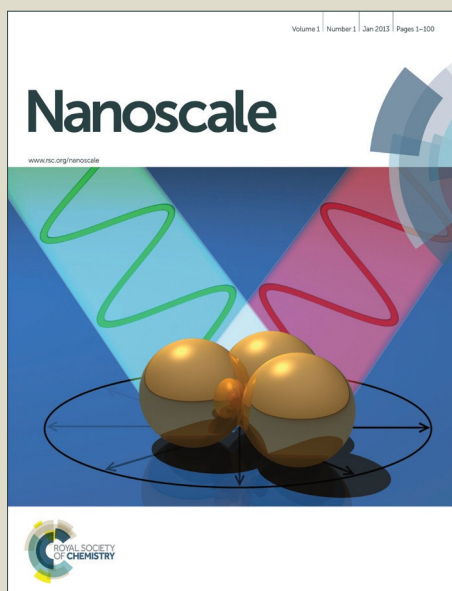


Nanoscale

Accepted Manuscript



This article can be cited before page numbers have been issued, to do this please use: M. Hadjidemetriou, Z. S. Al-Ahmady and K. Kostarelos, *Nanoscale*, 2016, DOI: 10.1039/C5NR09158F.



This is an *Accepted Manuscript*, which has been through the Royal Society of Chemistry peer review process and has been accepted for publication.

Accepted Manuscripts are published online shortly after acceptance, before technical editing, formatting and proof reading. Using this free service, authors can make their results available to the community, in citable form, before we publish the edited article. We will replace this *Accepted Manuscript* with the edited and formatted *Advance Article* as soon as it is available.

You can find more information about *Accepted Manuscripts* in the [Information for Authors](#).

Please note that technical editing may introduce minor changes to the text and/or graphics, which may alter content. The journal's standard [Terms & Conditions](#) and the [Ethical guidelines](#) still apply. In no event shall the Royal Society of Chemistry be held responsible for any errors or omissions in this *Accepted Manuscript* or any consequences arising from the use of any information it contains.

1
2
3 Time-evolution of *in vivo* protein corona onto blood-circulating
4 PEGylated liposomal doxorubicin (DOXIL) nanoparticles

5 Marilena Hadjidemetriou, Zahraa Al-Ahmady, Kostas Kostarelos*

6 *Nanomedicine Lab, School of Medicine, Faculty of Medical & Human Sciences and National Graphene Institute,*
7 *The University of Manchester, Manchester M13 9PT, United Kingdom*
8
9

10
11
12
13 **Abstract**

14 Nanoparticles (NPs) are instantly modified once injected in the bloodstream because of their
15 interaction with the blood components. The spontaneous coating of NPs by proteins, once in
16 contact with biological fluids, has been termed the 'protein corona' and it is considered to be
17 a determinant factor for the pharmacological, toxicological and therapeutic profile of NPs.
18 Protein exposure time is thought to greatly influence the composition of protein corona,
19 however the dynamics of protein interactions under realistic, *in vivo* conditions remain
20 unexplored. The aim of this study was to quantitatively and qualitatively investigate the time
21 evolution of *in vivo* protein corona, formed onto blood circulating, clinically used, PEGylated
22 liposomal doxorubicin. Protein adsorption profiles were determined 10 min, 1h and 3h post-
23 injection of liposomes into CD-1 mice. The results demonstrated that a complex protein
24 corona was formed as early as 10 min post-injection. Even though the total amount of
25 protein adsorbed did not significantly change over time, the fluctuation of protein
26 abundances observed indicated highly dynamic protein binding kinetics.

27
28 **Keywords:** protein corona, Doxil, time evolution, nanomedicine, nanoparticle, nanotoxicology
29
30
31
32
33
34
35
36
37

38
39 * Correspondence should be addressed to: kostas.kostarelos@manchester.ac.uk
40

41 ToC Graphic

42

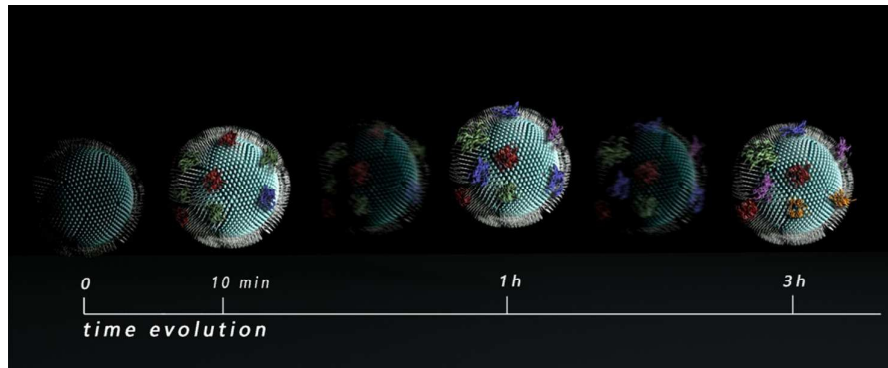
43

44

45

46

47



48

49 Highly dynamic binding kinetics of *in vivo* protein corona, formed onto PEGylated liposomal
50 doxorubicin nanoparticles after intravenous administration

51

52

53

54

55

56

57

58

59

60

61

62

63

64

65

66

67 Introduction

68 Nanoparticles (NPs) are thought to be instantly modified once injected in the bloodstream
69 because of their tendency to interact with the surrounding blood constituents, of which proteins have
70 been mostly studied today. The adsorption of proteins and their layering onto the surface of NPs has
71 been termed the 'protein corona'.¹ This bio-transformation of nanomaterials has been postulated as a
72 determinant factor for their overall biological behaviour and eventually their therapeutic efficacy.

73 The encapsulation of chemotherapeutic agents into phospholipid-based nanoscale vesicles,
74 called liposomes, has been the most clinically established strategy to reduce the toxicity to normal
75 tissues and simultaneously increase their accumulation into highly vascularised solid tumors.^{2,3}
76 Liposomal nanocarriers are being clinically used for more than 20 years, yet the effect of 'protein
77 corona' formation on liposomal pharmacology is scarcely studied and far from being well understood.
78 Despite the clinical use of liposomal doxorubicin (Doxil®)⁴ and the increased interest in the study of
79 serum protein corona formation around nanoparticles, there is currently no report in the literature
80 describing the identification of proteins adsorbed onto blood circulating doxorubicin-encapsulated
81 PEGylated liposomes. Such knowledge is needed not only to understand and predict liposomal
82 pharmacology, but also to improve the existing, clinically-used formulations, often displaying relatively
83 compromised therapeutic efficacy. The high-throughput proteomics analysis methods available today
84 are powerful tools to comprehensively study protein corona profiles of clinically used nanoparticles.

85 In addition to the physicochemical characteristics of NPs, protein exposure time is thought to
86 be a critical factor that shapes the composition of protein corona. The dynamics of protein interactions
87 with macroscale surfaces was first described by Vroman in 1962,⁵ suggesting a time-dependent
88 association and dissociation of proteins. According to this model, highly abundant proteins,
89 dominating at the early stage are later replaced by less abundant proteins with higher affinity for the
90 surface. This description, referred to as the 'Vroman effect', shaped the hypothesis that protein
91 corona formed onto the large surface area of NPs is a dynamic entity that evolves with time. There
92 have been several *in vitro* investigations into the time evolution of protein corona.⁶⁻⁸ Time-resolved
93 characterisation of *in vitro* protein corona was recently comprehensively investigated for silica and
94 polystyrene nanoparticles after the incubation with human plasma. In addition to 'Vroman' defined
95 binding kinetics, authors described the existence of more complex, 'peak' or 'cup' shaped binding
96 kinetics⁷. Despite the high-resolution quantitative LC-MS based proteomics employed and the insight
97 offered⁷, the limitation of these studies lies on the *in vitro* design of the interaction that fails to
98 recognize the highly dynamic nature of blood and its heterogeneous flow velocity.

99 In a recent report,⁹ we described a protocol to investigate the *in vivo* protein corona forming
100 onto three different types of blood circulating liposome types (bare, PEGylated and targeted). The
101 formation of *in vivo* protein corona was determined after the recovery of the liposomes from the blood
102 circulation of CD-1 mice 10 min post-injection, whereas *in vitro* protein corona was determined after
103 the incubation of liposomes in CD-1 mouse plasma. The differences between the protein coronas that
104 formed *in vitro* and *in vivo* were revealed for the first time. The molecular complexity and morphology
105 of the *in vivo* protein corona was shown not to be adequately predicted by the *in vitro* plasma
106 incubation of NPs. Even though the total amount of protein attached on circulating liposomes

107 correlated with that observed from *in vitro* incubations, the variety of molecular species in the *in vivo*
108 corona was considerably wider. However, one of the limitations of that study was that the liposome
109 systems studied (even though all constituted vesicles that have been clinically trialed) did not
110 encapsulate any therapeutic agent. In addition, due to the short half-life of bare (non-PEGylated)
111 liposomes employed, we chose to investigate corona formation at a single time point (10 min post-
112 incubation).

113 In this study, we attempted to investigate the time evolution of protein corona under realistic *in*
114 *vivo* conditions. Given the lack of protein corona investigations for clinically used liposomes, we
115 employed PEGylated liposomal doxorubicin, identical to the clinical product intravenously infused in
116 patients. The drug-loaded vesicles were injected into CD1 mice and recovered from the blood
117 circulation 10min, 1h and 3h post-injection. The protein coronas formed at these three different time
118 points were qualitatively and quantitatively characterized and compared (**Figure 1**).

119

120 Results and Discussion

121 The chemical composition and the physicochemical characteristics of doxorubicin-
122 encapsulated PEGylated liposomes that were fabricated for this study are summarized in **Table S1**.
123 The lipid composition and molar ratios of the individual lipid bilayer components were chosen to
124 match the exact liposome composition of the clinically-used liposomal doxorubicin agent Doxil®.
125 Dynamic light scattering (DLS), ζ -potential measurements and negative stain transmission electron
126 microscopy (TEM) were performed prior to intravenous administration of liposomes to access their
127 properties and morphology. Liposomes had a mean hydrodynamic diameter of 115 nm, a negative
128 surface charge of -36mV and displayed low polydispersity values (<0.06) indicating a narrow size
129 distribution (**Figure 2A**). TEM imaging showed well-dispersed, round shaped vesicles, with their size
130 correlating that of DLS measurements (**Figure 2B**; **Figure 2C**).

131 To obtain a time-dependent investigation of the *in vivo* formed protein corona, liposomes were
132 intravenously administered *via* tail vein injection into CD-1 mice and recovered by cardiac puncture
133 10min, 1h and 3h post-injection, as shown in **Figure 1**. Plasma was then prepared from recovered
134 blood by centrifugation (see Experimental section for further details). A protocol combining size
135 exclusion chromatography and membrane ultrafiltration was used for the isolation of liposome-corona
136 complexes from unbound and loosely bound plasma proteins, as previously described.⁹ This protocol
137 allows only the retention of the tightly adsorbed proteins onto the liposome surface, also referred by
138 some as the 'hard corona'.¹⁰

139 Dynamic light scattering measurements of protein corona-coated liposomes demonstrated
140 that their size distribution broadened (larger polydispersity index), while their surface charge remained
141 negative (**Figure 2A**; **Table S1**). In agreement with previous studies investigating liposomal protein
142 corona formation, we observed a blood-induced reduction in the mean diameter of liposomes,
143 consistent with all different time points of investigation (**Figure 2A**; **Table S1**).^{9, 11} This osmotically-
144 driven shrinkage was attributed to the high elastic deformation of liposomes, however it was also
145 observed here for doxorubicin-loaded vesicles without content loss as evidenced by cryo-EM (**Figure**

146 **2C**). In addition, TEM revealed well-dispersed liposomes that retained their structural integrity after
147 recovery, while the presence of the protein molecules adsorbed onto their surface revealed protein
148 corona formation, as early as 10 min-post injection (**Figure 2B and FigureS1**). In agreement with our
149 previous cryo-EM studies, the *in vivo* protein corona did not appear to coat all the available liposome
150 surfaces entirely⁹ (**Figure 2C**).

151 Based on established pharmacokinetic data for the clinically-used PEGylated liposomes
152 encapsulating doxorubicin,¹²⁻¹⁵ we knew that 40% of injected dose will remain in circulation for at least
153 6 hours. As a first step towards elucidation of the time evolution of the protein corona we
154 quantitatively compared the coronas formed around the drug-encapsulated PEGylated vesicles at
155 three different exposure times. To compare the total amount of protein adsorbed, we calculated the
156 protein binding ability (Pb), defined as the amount of protein associated with each μmole of lipid. As
157 shown in **Figure 3A**, Pb values determined at the earliest exposure time ($t=10\text{min}$) did not
158 significantly change even after the longest blood exposure time ($t=3\text{h}$). This data indicated that
159 liposome-specific protein fingerprints were already established by the earliest time point ($t=10\text{min}$)
160 and any possible qualitative changes in the composition of protein corona over time would be a result
161 of a competitive exchange process. Pb values observed for doxorubicin encapsulated liposomes,
162 were slightly higher than Pb values determined in our previous study for empty liposomes of the same
163 composition.⁹ This could be attributed to the different mass and blood flow dynamics of these vesicles
164 after the encapsulation of doxorubicin. Whether a second layer of proteins with low adherence,
165 sometimes termed as 'soft corona', exists or not remains to be proven and could not be resolved by
166 our analytical approach.

167 A comprehensive identification of proteins associated with liposomes was then performed by
168 mass spectrometry. The Venn diagram in **Figure 3B** illustrates the number of common and unique
169 proteins between the coronas formed after the three different time points of recovery. As already
170 evident from the quantification of total protein adsorbed (**Figure 3A**), a complex protein corona was
171 determined at the earliest time point ($t=10\text{ min}$), with 334 identified proteins (**Figure 3B**). The majority
172 of identified proteins ($n=180$) were common between the three time points. 90 unique proteins were
173 identified for the 10 min-formed corona, whereas 25 and 35 unique proteins were present in the
174 coronas of 1hr and 3hr recovered liposomes, respectively. It should be noted that the majority of
175 unique proteins belonged to the group of low abundance, as revealed by the Relative Protein
176 Abundance (RPA) values determined for each of the identified proteins. Previous *in vitro*
177 investigations suggested that protein corona reaches its final equilibrium 1hr post-incubation of NPs
178 with plasma proteins.⁶ Barran-Berdon *et al.* employed mass spectrometry to show that protein corona,
179 formed onto cationic liposomes incubated with human plasma, forms rapidly ($t=1\text{ min}$) and stops
180 evolving 1hr post-incubation.⁶ Our study demonstrated that the *in vivo* protein corona continues to
181 evolve over time, even at 3hr post-injection (**Figure 3B**). These contradictory results are not
182 surprising, considering the complexity of the physiological environment, the potential effect of blood
183 flow dynamics on the *in vivo* formation of the protein corona, as well as the role of possible NP-
184 triggered immune responses that may cause variations in the blood composition over time.

185 Pozzi D *et al.*,¹⁶ have previously showed that the *in vitro* incubation of empty liposomes with
186 fetal bovine serum (FBS) under static and flow conditions led to protein coronas of different
187 composition. Interestingly, dynamic (flow) conditions promoted the extensive adherence of low
188 molecular weight (MW) proteins, in comparison to incubation under static conditions. To investigate
189 whether the previous observation applies also under the more realistic, dynamic *in vivo* conditions of
190 blood flow, bound proteins were classified according to their molecular mass (**Figure 3C**). In
191 agreement with the study by Pozzi *et al.*,¹⁶ there was a tendency towards interaction with low MW
192 proteins. Plasma proteins with MW < 80 accounted for more than 80 % of the protein coronas formed
193 10min, 1hr and 3hr post-injection. Notably, a fluctuation in the contribution of each protein group
194 (classified based on MW) on the corona composition was observed over time. For instance, ~40% of
195 associated proteins had a MW < 20 at 10 min and 3hr time points, whereas the contribution of this
196 group was significantly lower 1hr post-injection (~25%), indicating the dynamic character of the *in vivo*
197 protein corona (**Figure 3C**).

198 To better understand the time evolution of the *in vivo* protein corona, the relative protein
199 abundance (RPA) of each identified protein was determined. **Figure 4A** summarizes the 20 most
200 abundant proteins associated with the surface of liposomes 10 min, 1hr and 3hr after their
201 intravenous administration. Blood exposure time was found to be a significant factor influencing
202 liposome-bound protein abundance. Common proteins observed in the Venn diagram of **Figure 3B**
203 were not equally abundant (**Figure 4**). A striking observation was that the most abundant protein of
204 the three coronas formed at different time points were not identical. Alpha-2 macroglobulin had the
205 highest RPA value 10min post-injection, while apolipoprotein E and hemoglobin beta-1 were the most
206 abundant proteins in the coronas of 1hr and 3hr blood-circulating liposomes, respectively.
207 Lipoproteins were found to be the most abundant class of proteins, contributing to ~20% of the 10
208 min-formed protein corona (**Figure 4B**), followed by immunoglobulins (RPA ~ 15%) and complement
209 proteins (RPA ~ 5%) (**Figure 4C**; **Figure 4D**).

210 Doxorubicin-encapsulated, PEGylated liposomes, employed in this study, were designed to
211 have a prolonged blood circulation half-life which enhances their possibility to extravasate through the
212 leaky tumor vasculature.² There have been several proposed mechanisms to explain the prolonged
213 circulation of PEGylated nanovehicles. In agreement with previous reports, this study demonstrated
214 that PEGylated surfaces are not completely inert and interact with the blood components *in vivo*.¹⁷⁻¹⁹
215 Even though PEGylation reduced the total amount of proteins adsorbed,⁹ the presence of opsonins
216 (complement proteins and immunoglobulins) in their protein coronas (**Figure 4**) may be thought to
217 contradict with their long-circulating profile. The concept of 'dys-opsonization' has been proposed to
218 describe the adsorption of proteins that extend the circulation time of liposomes.²⁰ Lipoproteins
219 identified in this study as the most abundant proteins (**Figure 4B**), have been suggested to have dys-
220 opsonic activity, possibly explained by their competitive binding with opsonic proteins. Also, the PEG-
221 mediated inhibition of liposome interaction with circulating cells has been suggested, based on
222 previous *in vitro* studies reporting reduced internalization of liposomes after PEGylation²¹. According
223 to this scenario, the identity of the protein corona seems to have a minor impact on the overall
224 biodistribution profile of PEGylated liposomes.

225 As illustrated in **Figure 4D**, the *in vivo* protein coronas formed at the three different time
226 points, consisted of several key complement cascade proteins, involved in the classical (complement
227 C1q, C4b), alternative (complement factor h) and lectin (mannan-binding lectin serine protease,
228 mannan-binding lectin) pathways of activation.²² The impact of complement activation on the
229 potential adverse effects of liposomes had been valued before the term 'protein corona' was
230 introduced.²³ Immediately after intravenous infusion, PEGylated liposomal doxorubicin has been
231 previously shown to interact with the complement system causing transient and in most of the cases
232 mild hypersensitive reactions, termed as C-activation related pseudoallergy (CARPA).^{24, 25} Chanan-
233 Khan *et al.* reported that 45% of cancer patients (n=29) treated for the first time with Doxil
234 experienced hypersensitivity reactions associated by complement activation.²⁴ Plasma levels of
235 protein-s bound C terminal complex (SC5B-9) have been traditionally used as an indicator of
236 complement activation.²⁴ However, correlations between material properties and complement
237 activation were difficult to be made without thorough identification of adhered proteins. *In vivo* protein
238 corona fingerprinting offers a new tool for molecular investigation of nanoparticle-triggered
239 complement events and the consequences arising from them and more work would be needed to
240 explore this further. However, it is also important to appreciate the potential limitations of extrapolating
241 immune system data from mice to humans.²⁶

242 To gain some further understanding of the protein binding kinetics occurring *in vivo* after the
243 intravenous administration of NPs, we classified the most abundant liposome-bound proteins into 5
244 groups according to the fluctuation of their normalized protein abundance value over time (**Figure**
245 **S2**). In agreement with the 'Vroman effect' theory, some proteins replaced or were replaced by others
246 exhibiting increased (**Figure S2A**) or reduced (**Figure S2B**) binding over time, respectively. For
247 instance, the abundance of fibrinogen in the protein corona formed 3hr post-injection was 5 times
248 greater in comparison with the abundance observed for the 10min-formed corona. Tenzer and co-
249 workers were the first to describe the existence of more complex, 'peak' or 'cup' shaped binding
250 kinetics after the *in vitro* incubation of silica and polystyrene NPs with human plasma.⁷ Similarly, we
251 observed proteins characterized by low abundance at the beginning of blood circulation (t=10min) and
252 at later time points (t=3hr), but displaying peak abundance at intermediate time points (t=1hr) (**Figure**
253 **S2C**) or *vice versa* (**Figure S2D**). In addition to the above mentioned binding kinetic groups we also
254 observed proteins that retained their abundance over time (**Figure S2E**). The sum of all the binding
255 kinetic processes observed, resulted in a constant total amount of protein on the surface of liposomes
256 over time (Figure 2A). Such observations are of great importance to comprehensively understand the
257 overall performance of already clinically established formulations. We have previously shown that
258 almost 40% and 15% of the injected liposomal doxorubicin remains in the blood after 6 h and 24 h,
259 respectively.¹³ This suggests that liposomes extravasate at the tumor tissue at different time points
260 post-injection. It has been also shown that the drug release profiles,²⁷ as well as the interaction of
261 liposomes with cells,^{28, 29} are greatly affected by the proteins adsorbed onto their surfaces. Therefore,
262 the *in vivo*, highly dynamic protein binding kinetics, demonstrated in this study, could result in altered
263 therapeutic efficacy of liposomes over time

264 On a broader context, we propose that understanding the biological impact of *in vivo* forming
265 protein corona is crucial for the rational design of new formulations, with improved therapeutic
266 efficacy. Much work has been done concerning the effect of protein corona on the interaction of NPs
267 with cells, suggesting that protein adsorption can either facilitate³⁰ or inhibit³¹ cellular uptake. The
268 observation that the targeting capabilities of nanoscale constructs are diminished while in blood
269 circulation because of their interaction with plasma proteins³¹ has also led to the idea of exploiting the
270 protein corona in order to direct them to specific target cells. According to this strategy, NPs can be
271 specifically designed to interact with proteins that will initiate targeted receptor mediated
272 endocytosis.³⁰ However, a comprehensive characterization of protein corona under physiological
273 conditions is necessary before exploring its potential exploitation for targeting purposes. Blood flow
274 dynamics, although a great influential factor for nanoparticle-protein interactions, seem to be largely
275 ignored in the protein corona literature. In our previous study, we demonstrated that the complexity of
276 *in vivo* formed protein corona cannot be adequately predicted by *in vitro* plasma incubations.⁹ In
277 addition, data in this study suggest that *in vivo* characterization of the protein corona at a single time
278 point is insufficient to describe the surface modifications that nanoparticles experience *in vivo*. The
279 fluctuation in the abundance of each identified protein, observed over time, reveals that the formation
280 of protein corona in a controlled and predictable manner, as often suggested, is challenging, if not
281 physiologically unrealistic.

282

283 Conclusion

284 This is the first study to investigate the time evolution of protein corona under realistic *in vivo*
285 conditions. Protein adsorption profiles were determined at three different time points post-injection
286 (10min, 1hr and 3hr) of PEGylated liposomal doxorubicin, clinically used for the treatment of various
287 neoplastic conditions. The results demonstrated that a complex protein corona was formed as early
288 as 10min post-injection. Even though the total amount of protein adsorbed did not significantly
289 change, the abundance of each protein identified fluctuated over time indicating that competitive
290 exchange processes were taking place. We anticipate that comprehensive identification of protein
291 coronas under realistic *in vivo* conditions for different types of blood-injected pharmacological agents
292 that lie in the nanoscale is necessary to improve our understanding of their overall clinical
293 performance.

294

295

296

297

298

299

300 Experimental

301 Materials

302 Hydrogenated soy phosphatidylcholine (HSPC), 1,2-distearoyl-sn-glycero-3-phosphoethanolamine-
303 N-[methoxy(polyethylene glycol)-2000 (DSPE-PEG2000) and 1,2-distearoyl-sn-glycero-3-
304 phosphoethanolamine-N-[maleimide(polyethylene glycol)-2000] (ammonium salt) (Mal-DSPE-
305 PEG2000) were purchased from Avanti Polar Lipids (USA), while doxorubicin hydrochloride,
306 cholesterol and 4-(2-Hydroxyethyl) piperazine-1-ethanesulfonic acid (HEPES) were purchased from
307 Sigma (UK).

308 Preparation of PEGylated liposomal doxorubicin nanoparticles

309 Liposomes were prepared by thin lipid film hydration method followed by extrusion. **Table S1** shows
310 the liposomal formulation employed, the lipid composition and the molar ratios. Briefly, lipids of
311 different types were dissolved in chloroform:methanol mixture (4:1) in a total volume of 2 ml, using a
312 25 ml round bottom flask. Organic solvents were then evaporated using a rotary evaporator (Buchi,
313 Switzerland) at 40 °C, at 150 rotations /min, 1 h under vacuum. Lipid films were hydrated with
314 ammonium sulphate 250 mM (pH 8.5) at 60 °C to produce large multilamellar liposomes. Small
315 unilamellar liposomes were then produced by extrusion through 800 nm and 200 nm polycarbonate
316 filters (Whatman, VWR, UK) 10 times each and then 15 times through 100 nm and 80 nm extrusion
317 filters (Whatman, VWR, UK) using a mini-Extruder (Avanti Polar Lipids, Alabaster, AL).

318 For DOX loading, the ammonium sulphate gradient method was used. Exchanging the external
319 unencapsulated ammonium sulphate was performed by gel filtration through Sepharose CL-4B
320 column (15 cm x 1.5 cm) (Sigma, UK) equilibrated with HBS (pH 7.4). Doxorubicin hydrochloride was
321 added to the liposome suspensions at 1:20 DOX:Lipids mass ratio in respect to the original total lipid
322 concentration. Subsequently, samples were incubated at 60 °C for 1h. After incubation, liposomes
323 were passed through PD-10 desalting columns (GE Healthcare Life Sciences) to remove any free
324 DOX.

325 Animal experiments

326 Eight to ten week old female CD1 mice were purchased from Charles River (UK). Animal procedures
327 were performed in compliance with the UK Home Office Code of Practice for the Housing and Care of
328 Animals used in Scientific Procedures. Mice were housed in groups of five with free access to water
329 and kept at temperature of 19-22 °C and relative humidity of 45-65%. Before performing the
330 procedures, animals were acclimatized to the environment for at least 7 days.

331 Protein corona formation after *in vivo* administration

332 CD1 mice were anesthetized by inhalation of isoflurane and liposomes were administered
333 intravenously *via* the lateral tail vein, at a lipid dose of 0.125mM/g body weight to achieve a final
334 doxorubicin dose of 5mg/kg body weight, used for preclinical studies.³²⁻³⁴ 10 minutes, 1h and 3h post-
335 injection, blood was recovered by cardiac puncture using K2EDTA coated blood collection tubes.
336 Approximately 0.5-1ml of blood was recovered from each mouse. Plasma was prepared by inverting
337 10 times the collection tubes to ensure mixing of blood with EDTA and subsequent centrifugation for
338 12 minutes at 1300 RCF at 4 °C. Supernatant was collected into Protein LoBind Eppendorf Tubes.
339 For each time point the plasma samples obtained from three mice were pooled together for a final
340 plasma volume of 1 ml. Three experimental replicates were performed and therefore 9 mice were
341 used in total for each time point.

342 Separation of corona-coated liposomes from unbound and weakly bound proteins

343 Liposomes recovered from *in vivo* experiments were separated from excess plasma proteins by size
344 exclusion chromatography followed by membrane ultrafiltration, as we have previously described.⁹
345 Immediately after the *in vivo* incubations, 1ml of plasma samples was loaded onto a Sepharose CL-
346 4B (SIGMA-ALDRICH) column (15x1.5cm) equilibrated with HBS. Chromatographic fractions 4,5 and
347 6 containing liposomes were then pooled together and concentrated to 500 µl by centrifugation using
348 Vivaspin 6 column (10000 MWCO, Sartorius, Fisher Scientific) at 3000rpm. Vivaspin 500 centrifugal
349 concentrator (1 000 000 MWCO, Sartorius, Fisher Scientific) was then used at 3000 rpm, to further
350 concentrate the samples to 100 µl and to ensure separation of protein-coated liposomes from the
351 remaining large unbound proteins. Liposomes were then washed 3 times with 100 µl HBS to remove
352 weakly bound proteins.

353

359 Size and zeta potential measurements using dynamic light scattering (DLS)

360 Liposome size and surface charge were measured using Zetasizer Nano ZS (Malvern, Instruments,
361 UK). For size measurement, samples were diluted with distilled water in 1 ml cuvettes. Zeta potential
362 was measured in disposable Zetasizer cuvettes and sample dilution was performed with distilled
363 water. Size and zeta potential data were taken in three and five measurements, respectively

364

365 Transmission electron microscopy (TEM)

366 Liposomes of different compositions were visualized with transmission electron microscopy (FEI
367 Tecnai 12 BioTwin) before and after their *in vivo* interaction with plasma proteins. Samples were
368 diluted to 1 mM lipid concentration, then a drop from each liposome suspension was placed onto a
369 Carbon Film Mesh Copper Grid (CF400-Cu, Electron Microscopy Science) and the excess
370 suspension was removed with a filter paper. Staining was performed using aqueous uranyl acetate
371 solution 1%.

372

373 Cryo-electron microscopy

374 TEM grids of liposomes were prepared in a FEI Vitrobot using 3 μ l of sample absorbed to freshly glow-
375 discharged R2/2 Quantifoil grids. Grids were continuously blotted for 4–5 s in a 95% humidity
376 chamber before plunge-freezing into liquid ethane. Data were then recorded on a Polara F30 FEG
377 operating at 200 kV on a 4K Gatan Ultrascan CCD (charge-coupled device) in low-dose mode. CD
378 images were recorded between 0.5 and 5.0 μ m defocus at a normal magnification of 39,000 x and at
379 3.5 $\text{\AA}/\text{pixel}$ (1 \AA = 0.1 nm) and had a maximum electron dose of <25 electrons/ \AA^2 .

380

381 Quantification of adsorbed proteins

382 Proteins associated with recovered liposomes were quantified by BCA Protein assay kit. Pb values,
383 expressed as μ g of protein/ μ M lipid were then calculated and represented as the average \pm standard
384 error of three independent experiments. For the BCA assay, a 6-point standard curve was generated
385 by serial dilutions of BSA in HBS, with the top standard at a concentration of 2 μ g/ml. BCA reagent A
386 and B were mixed at a ratio of 50:1 and 200 μ l of the BCA mixture were dispensed into a 96-well plate,
387 in duplicates. Then, 25 μ l of each standard or unknown sample were added per well. The plate was
388 incubated for 30 minutes at 37°C, after which the absorbance was read at 574nm on a plate reader
389 (Fluostar Omega). Protein concentrations were calculated according to the standard curve. To
390 quantify lipid concentration, 20 μ l of each samples was mixed with 1ml of chloroform and 500 μ l of
391 Stewart assay reagent in an Eppendorf tube. The samples were vortexed for 20 seconds followed by
392 1 min of centrifugation at 13 000 RPM. 200 μ l of the chloroform phase was transferred to a quartz
393 cuvette. The optical density was measured on a using Cary 50 Bio Spectrophotometer (Agilent
394 Technologies) at 485 nm. Lipid concentration was calculated according to a standard curve.

395

396 Mass Spectrometry

397 Proteins associated with 0.05 μ M of liposomes were mixed with Protein Solving Buffer (Fisher
398 Scientific) for a final volume of 25 μ l and boiled for 5 minutes at 90°C. Samples were then loaded in
399 10% Precise Tris-HEPES Protein Gel (Thermo Scientific). The gel was run for 3-5 minutes 100V, in
400 50 times diluted Tris-HEPES SDS Buffer (Thermo Scientific). Staining was performed with EZ Blue™
401 Gel Staining reagent (Sigma Life Science) overnight followed by washing in distilled water for 2 h.
402 Bands of interest were excised from the gel and dehydrated using acetonitrile followed by vacuum
403 centrifugation. Dried gel pieces were reduced with 10 mM dithiothreitol and alkylated with 55
404 mM iodoacetamide. Gel pieces were then washed alternately with 25 mM ammonium bicarbonate
405 followed by acetonitrile. This was repeated, and the gel pieces dried by vacuum
406 centrifugation. Samples were digested with trypsin overnight at 37°C.

407

408 Digested samples were analysed by LC-MS/MS using an UltiMate® 3000 Rapid Separation LC
409 (RSLC, Dionex Corporation, Sunnyvale, CA) coupled to Orbitrap Velos Pro (Thermo Fisher
410 Scientific) mass spectrometer. Peptide mixtures were separated using a gradient from 92% A (0.1%
411 FA in water) and 8% B (0.1% FA in acetonitrile) to 33% B, in 44 min at 300 nL min⁻¹, using a 250 mm
412 x 75 μ m i.d. 1.7 μ M BEH C18, analytical column (Waters). Peptides were selected for fragmentation
413 automatically by data dependant analysis. Data produced were searched using Mascot (Matrix
414 Science UK), against the [Uniprot] database with taxonomy of [mouse] selected. Data were validated
415 using Scaffold (Proteome Software, Portland, OR).

416

417 The Scaffold software (version 4.3.2, Proteome Software Inc.) was used to validate MS/MS based
418 peptide and protein identifications and for relative quantification based on spectral counting. Peptide

419 identifications were accepted if they could be established at greater than 95.0% probability by the
420 Peptide Prophet algorithm with Scaffold delta-mass correction. Protein identifications were accepted if
421 they could be established at greater than 99.0% probability and contained at least 2 identified
422 peptides. Protein probabilities were assigned by the Protein Prophet algorithm. Proteins that
423 contained similar peptides and could not be differentiated based on MS/MS analysis alone were
424 grouped to satisfy the principles of parsimony. Semi quantitative assessment of the protein amounts
425 was conducted using normalized spectral countings, NSCs, provided by Scaffold Software. The mean
426 value of NSCs obtained in the three experimental replicates for each protein was normalized to the
427 protein MW and expressed as a relative quantity by applying the following equation:¹⁷

$$\text{MWNSC}_k = \frac{(\text{NSC}/\text{MW})_k}{\sum_{i=1}^N (\text{NSC}/\text{MW})_i} \times 100 \quad (1)$$

428

429 where, MWNSC_k is the percentage molecular weight normalized NSC for protein k and MW is the
430 molecular weight in kDa for protein k. This equation takes into consideration the protein size and
431 evaluates the contribution of each protein reflecting its relative protein abundance (RPA).

432

433 **Statistical Analysis**

434 Statistical analysis of the data was performed using IBM SPSS Statistics software. One-way analysis
435 of variance (ANOVA) followed by the Tukey multiple comparison test were used and p values < 0.05
436 were considered significant.

437

438

439

440 **Conflict of Interest**

441 The authors declare no competing financial interest.

442

443

444 **Acknowledgments**

445 This research was partially funded by the Marie Curie Initial Training Network *PathChooser* (PITN-GA-2013-
446 608373). The authors also wish to thank the staff in the Faculty of Life Sciences EM Facility for their assistance
447 and the Wellcome Trust for equipment grant support to the EM Facility. In addition, Mass Spectrometry Facility
448 staff at the University of Manchester for their assistance and Mr. M.Sylianides for his help with the TOC image
449 and liposome illustration.

450

451 **Author contributions**

452 M.Hadjidemetriou designed and performed all experiments and took responsibility for planning and writing the
453 manuscript. Z.Al-ahmady contributed in the intravenous administration of liposomes and blood collection.
454 K.Kostarelos initiated, designed, directed, provided intellectual input and contributed to the writing of the
455 manuscript.

456

457

458

459

460

461

462

463

464

References

- 465 1. Cedervall, T.; Lynch, I.; Lindman, S.; Berggard, T.; Thulin, E.; Nilsson, H.; Dawson, K. A.; Linse, S., Understanding the
466 nanoparticle-protein corona using methods to quantify exchange rates and affinities of proteins for nanoparticles.
467 *Proceedings of the National Academy of Sciences of the United States of America* 2007, 104, 2050-2055.
- 468 2. Laginha, K. M.; Verwoert, S.; Charrois, G. J.; Allen, T. M., Determination of doxorubicin levels in whole tumor and tumor
469 nuclei in murine breast cancer tumors. *Clinical cancer research : an official journal of the American Association for Cancer
470 Research* 2005, 11, 6944-9.
- 471 3. Safra, T.; Muggia, F.; Jeffers, S.; Tsao-Wei, D. D.; Groshen, S.; Lyass, O.; Henderson, R.; Berry, G.; Gabizon, A.,
472 Pegylated liposomal doxorubicin (doxil): reduced clinical cardiotoxicity in patients reaching or exceeding cumulative doses
473 of 500 mg/m². *Ann Oncol* 2000, 11, 1029-33.
- 474 4. Barenholz, Y., Doxil(R)—the first FDA-approved nano-drug: lessons learned. *J Control Release*. 2012, 160, 117-34.
- 475 5. Vroman, L., Effect of Adsorbed Proteins on Wettability of Hydrophilic and Hydrophobic Solids. *Nature* 1962, 196, 476-8.
- 476 6. Barran-Berdon, A. L.; Pozzi, D.; Caracciolo, G.; Capriotti, A. L.; Caruso, G.; Cavaliere, C.; Riccioli, A.; Palchetti, S.; Lagana,
477 A., Time evolution of nanoparticle-protein corona in human plasma: relevance for targeted drug delivery. *Langmuir : the
478 ACS journal of surfaces and colloids* 2013, 29, 6485-94.
- 479 7. Tenzer, S.; Docter, D.; Kuharev, J.; Musyanovych, A.; Fetz, V.; Hecht, R.; Schlenk, F.; Fischer, D.; Kiouptsi, K.; Reinhardt,
480 C.; Landfester, K.; Schild, H.; Maskos, M.; Knauer, S. K.; Stauber, R. H., Rapid formation of plasma protein corona critically
481 affects nanoparticle pathophysiology. *Nat. nanotechnol.* 2013, 8, 772-81.
- 482 8. Casals, E.; Pfaller, T.; Duschl, A.; Oostingh, G. J.; Püntes, V., Time Evolution of the Nanoparticle Protein Corona. *ACS
483 nano* 2010, 4, 3623-3632.
- 484 9. Hadjidemetriou, M.; Al-Ahmady, Z.; Mazza, M.; Collins, R. F.; Dawson, K.; Kostarelos, K., In Vivo Biomolecule Corona
485 around Blood-Circulating, Clinically Used and Antibody-Targeted Lipid Bilayer Nanoscale Vesicles. *ACS nano* 2015, 9,
486 8142-56.
- 487 10. Monopoli, M. P.; Aberg, C.; Salvati, A.; Dawson, K. A., Biomolecular coronas provide the biological identity of nanosized
488 materials. *Nature nanotechnology* 2012, 7, 779-86.
- 489 11. Wolfram, J.; Suri, K.; Yang, Y.; Shen, J.; Celia, C.; Fresta, M.; Zhao, Y.; Shen, H.; Ferrari, M., Shrinkage of pegylated and
490 non-pegylated liposomes in serum. *Colloids and surfaces. B, Biointerfaces* 2014, 114, 294-300.
- 491 12. Gabizon, A.; Shmeeda, H.; Barenholz, Y., Pharmacokinetics of pegylated liposomal Doxorubicin: review of animal and
492 human studies. *Clinical pharmacokinetics* 2003, 42, 419-36.
- 493 13. Al-Jamal, W. T.; Al-Ahmady, Z. S.; Kostarelos, K., Pharmacokinetics & tissue distribution of temperature-sensitive liposomal
494 doxorubicin in tumor-bearing mice triggered with mild hyperthermia. *Biomaterials* 2012, 33, 4608-17.
- 495 14. Al-Ahmady, Z. S.; Scudamore, C. L.; Kostarelos, K., Triggered doxorubicin release in solid tumors from thermosensitive
496 liposome-peptide hybrids: Critical parameters and therapeutic efficacy. *Int J Cancer* 2015, 137, 731-43.
- 497 15. Al-Ahmady, Z. S.; Chaloin, O.; Kostarelos, K., Monoclonal antibody-targeted, temperature-sensitive liposomes: in vivo
498 tumor chemotherapeutics in combination with mild hyperthermia. *Journal of controlled release : official journal of the
499 Controlled Release Society* 2014, 196, 332-43.
- 500 16. Pozzi, D.; Caracciolo, G.; Digiaco, L.; Colapicchioni, V.; Palchetti, S.; Capriotti, A. L.; Cavaliere, C.; Zenezini Chiozzi, R.;
501 Puglisi, A.; Lagana, A., The biomolecular corona of nanoparticles in circulating biological media. *Nanoscale* 2015, 7, 13958-
502 66.
- 503 17. Pozzi, D.; Colapicchioni, V.; Caracciolo, G.; Piovesana, S.; Capriotti, A. L.; Palchetti, S.; De Grossi, S.; Riccioli, A.;
504 Amenitsch, H.; Lagana, A., Effect of polyethyleneglycol (PEG) chain length on the bio-nano-interactions between
505 PEGylated lipid nanoparticles and biological fluids: from nanostructure to uptake in cancer cells. *Nanoscale* 2014, 6, 2782-
506 92.
- 507 18. Dobrovolskaia, M. A.; Neun, B. W.; Man, S.; Ye, X.; Hansen, M.; Patri, A. K.; Crist, R. M.; McNeil, S. E., Protein corona
508 composition does not accurately predict hematocompatibility of colloidal gold nanoparticles. *Nanomedicine* 2014, 10, 1453-
509 63.
- 510 19. Gref, R.; Luck, M.; Quellec, P.; Marchand, M.; Dellacherie, E.; Harnisch, S.; Blunk, T.; Muller, R. H., 'Stealth' corona-core
511 nanoparticles surface modified by polyethylene glycol (PEG): influences of the corona (PEG chain length and surface
512 density) and of the core composition on phagocytic uptake and plasma protein adsorption. *Colloids Surf., B* 2000, 18, 301-
513 313.
- 514 20. Moghimi, S. M.; Muir, I. S.; Illum, L.; Davis, S. S.; Kolb-Bachofen, V., Coating particles with a block co-polymer
515 (poloxamine-908) suppresses opsonization but permits the activity of dysopsonins in the serum. *Biochimica et biophysica
516 acta* 1993, 1179, 157-65.
- 517 21. Mishra, S.; Webster, P.; Davis, M. E., PEGylation significantly affects cellular uptake and intracellular trafficking of non-viral
518 gene delivery particles. *European journal of cell biology* 2004, 83, 97-111.
- 519 22. Fujita, T., Evolution of the lectin-complement pathway and its role in innate immunity. *Nature reviews. Immunology* 2002, 2,
520 346-53.
- 521 23. Szebeni, J., Complement activation-related pseudoallergy: a new class of drug-induced acute immune toxicity. *Toxicology*
522 2005, 216, 106-21.
- 523 24. Chanan-Khan, A.; Szebeni, J.; Savay, S.; Liebes, L.; Rafique, N. M.; Alving, C. R.; Muggia, F. M., Complement activation
524 following first exposure to pegylated liposomal doxorubicin (Doxil): possible role in hypersensitivity reactions. *Ann Oncol*
525 2003, 14, 1430-7.
- 526 25. Szebeni, J.; Muggia, F.; Gabizon, A.; Barenholz, Y., Activation of complement by therapeutic liposomes and other lipid
527 excipient-based therapeutic products: prediction and prevention. *Advanced drug delivery reviews* 2011, 63, 1020-30.
- 528 26. Caracciolo, G.; Pozzi, D.; Capriotti, A. L.; Cavaliere, C.; Piovesana, S.; La Barbera, G.; Amici, A.; Lagana, A., The
529 liposome-protein corona in mice and humans and its implications for in vivo delivery. *J. Mater. Chem. B* 2014, 2, 7419-
530 7428.
- 531 27. Behzadi, S.; Serpooshan, V.; Sakhtianchi, R.; Muller, B.; Landfester, K.; Crespy, D.; Mahmoudi, M., Protein corona change
532 the drug release profile of nanocarriers: the "overlooked" factor at the nanobio interface. *Colloids and surfaces. B,
533 Biointerfaces* 2014, 123, 143-9.

- 534 28. Caracciolo, G.; Callipo, L.; De Sanctis, S. C.; Cavaliere, C.; Pozzi, D.; Lagana, A., Surface adsorption of protein corona
535 controls the cell internalization mechanism of DC-Chol-DOPE/DNA lipoplexes in serum. *Biochimica et biophysica acta*
536 2010, 1798, 536-43.
- 537 29. Hadjidemetriou, M.; Pippa, N.; Pispas, S.; Dernetzos, C., Incorporation of dimethoxycurcumin into charged liposomes and
538 the formation kinetics of fractal aggregates of uncharged vectors. *Journal of Liposome Research* 2013, 23, 94-100.
- 539 30. Caracciolo, G.; Cardarelli, F.; Pozzi, D.; Salomone, F.; Maccari, G.; Bardi, G.; Capriotti, A. L.; Cavaliere, C.; Papi, M.;
540 Lagana, A., Selective targeting capability acquired with a protein corona adsorbed on the surface of 1,2-dioleoyl-3-
541 trimethylammonium propane/DNA nanoparticles. *ACS applied materials & interfaces* 2013, 5, 13171-9.
- 542 31. Salvati, A.; Pitek, A. S.; Monopoli, M. P.; Prapainop, K.; Bombelli, F. B.; Hristov, D. R.; Kelly, P. M.; Aberg, C.; Mahon, E.;
543 Dawson, K. A., Transferrin-functionalized nanoparticles lose their targeting capabilities when a biomolecule corona adsorbs
544 on the surface. *Nat. Nanotechnol.* 2013, 8, 137-143.
- 545 32. Al-Ahmady, Z. S.; Al-Jamal, W. T.; Bossche, J. V.; Bui, T. T.; Drake, A. F.; Mason, A. J.; Kostarelos, K., Lipid-peptide
546 vesicle nanoscale hybrids for triggered drug release by mild hyperthermia in vitro and in vivo. *ACS Nano* 2012, 6, 9335-46.
- 547 33. Needham, D.; Anyarambhatla, G.; Kong, G.; Dewhirst, M. W., A new temperature-sensitive liposome for use with mild
548 hyperthermia: characterization and testing in a human tumor xenograft model. *Cancer research* 2000, 60, 1197-201.
- 549 34. Kong, G.; Anyarambhatla, G.; Petros, W. P.; Braun, R. D.; Colvin, O. M.; Needham, D.; Dewhirst, M. W., Efficacy of
550 liposomes and hyperthermia in a human tumor xenograft model: importance of triggered drug release. *Cancer Research*
551 2000, 60, 6950-7.

552

553

554

555 **Figure Legends**

556 **Figure1: Schematic description of the experimental design.** To obtain a time-dependent
557 investigation of the *in vivo* formed protein corona (PC), liposomes were intravenously administered *via*
558 tail vein injection into CD-1 mice (n=3 mice / group; 3 independent experiments replicated) and
559 recovered by cardiac puncture 10min, 1h and 3h post-injection. The plasma was then separated from
560 the recovered blood by centrifugation. *In vivo* protein-coated liposomes were purified from unbound
561 proteins and protein coronas formed at these three different time points were qualitatively and
562 quantitatively characterized and compared.

563
564 **Figure 2: The effect of protein corona formation on the physicochemical characteristics and**
565 **morphology of liposomes. (A)** Mean diameter (nm) and ζ -potential (mV) distributions and **(B)**
566 Negative stain TEM imaging of liposomes before their interaction with plasma proteins and **10 min,**
567 **1h** and **3h** after their i.v. injection and recovery from CD-1 mice. **(C)** Cryo-EM imaging of doxorubicin-
568 encapsulating (white arrow) liposomes before injection and recovered after 10 min in blood
569 circulation, partially coated with plasma proteins (black arrow). All scale bars are 100nm.

570 **Figure 3: Characterization of *in vivo* protein corona: (A)** Comparison of the total amount of
571 proteins adsorbed *in vivo* onto liposomes recovered from CD1 mouse circulation 10 min, 1h and 3h
572 post-injection. Pb values (μg of protein/ μM lipid) represent the average and standard error from three
573 independent experiments, each using three-six mice; **(B)** Venn diagrams report the number of unique
574 proteins identified in the *in vivo* corona formed 10 min, 1h and 3h post-injection and their respective
575 overlap; **(C)** Classification of the corona proteins identified according to their molecular mass.

576 **Figure 4: Time evolution of *in vivo* protein corona: (A)** Most-abundant proteins (top-20) identified
577 in the protein corona of PEGylated liposomal doxorubicin 10 min, 1h and 3h post-injection by LC-
578 MS/MS. Relative protein abundance (RPA) values represent the average and standard error from
579 three independent experiments; **(B)** The relative percentage of lipoproteins, immunoglobulins and
580 complement proteins identified in the protein corona 10 min, 1h and 3h post-injection.

581

582

583 **Supporting Figure Legends**

584 **Table S1: The physicochemical characteristics of PEGylated liposomal doxorubicin before and**
585 **after extraction from blood circulation.** Mean vesicle diameter (nm) and ζ -potential (mV) data from
586 DLS and surface charge electrophoresis are shown.

587 **FigureS1:** Negative stain TEM imaging of liposomes before their interaction with plasma proteins and
588 **10 min, 1h** and **3h** after their i.v. injection and recovery from CD-1 mice. Arrows show the presence of
589 proteins around the surface of liposomes. All scale bars are 50nm.

590 **Figure S2: Protein binding kinetics during corona evolution.** Relative values were normalized to
591 the maximum amount (set to 1) across the three time points for each of the top-20 proteins. Corona
592 proteins were classified into five groups: **(A)** Proteins displaying increased binding over time; **(B)**
593 Proteins displaying reduced binding over time **(C)** Proteins characterized by low abundance at the
594 early (t=10min) and late time points (t=3h) and higher abundance at intermediate time point (t=1h);
595 **(D)** Proteins characterized by high abundance at the early (t=10min) and late time points (t=3h) and
596 lower abundance at intermediate time point (t=1h); **(E)** Proteins with constant abundance over time.

597

598

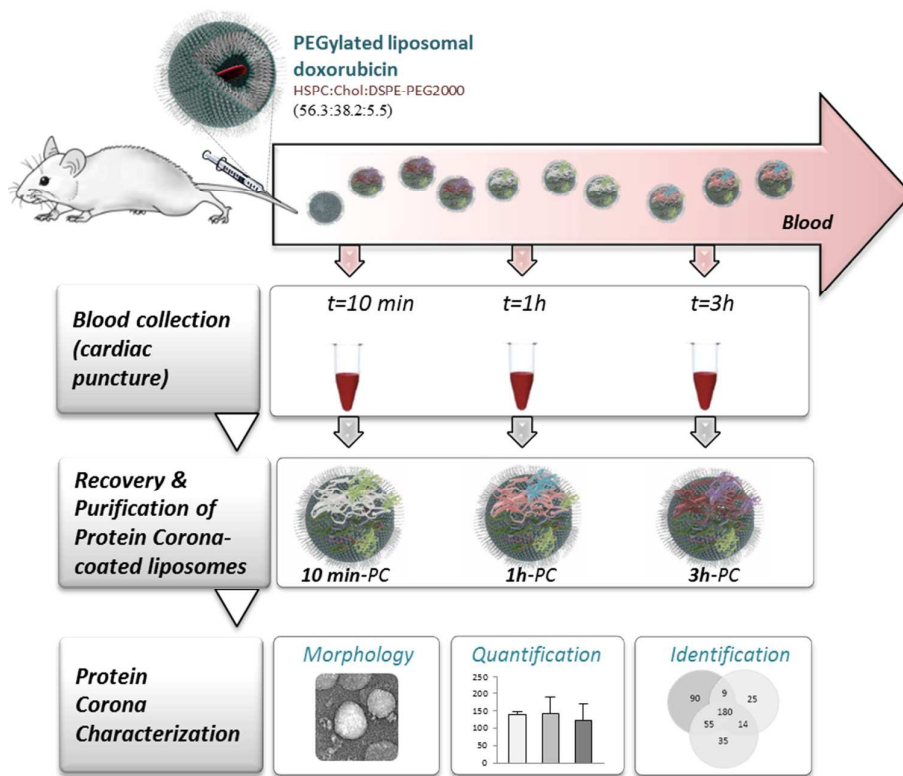


Figure 1

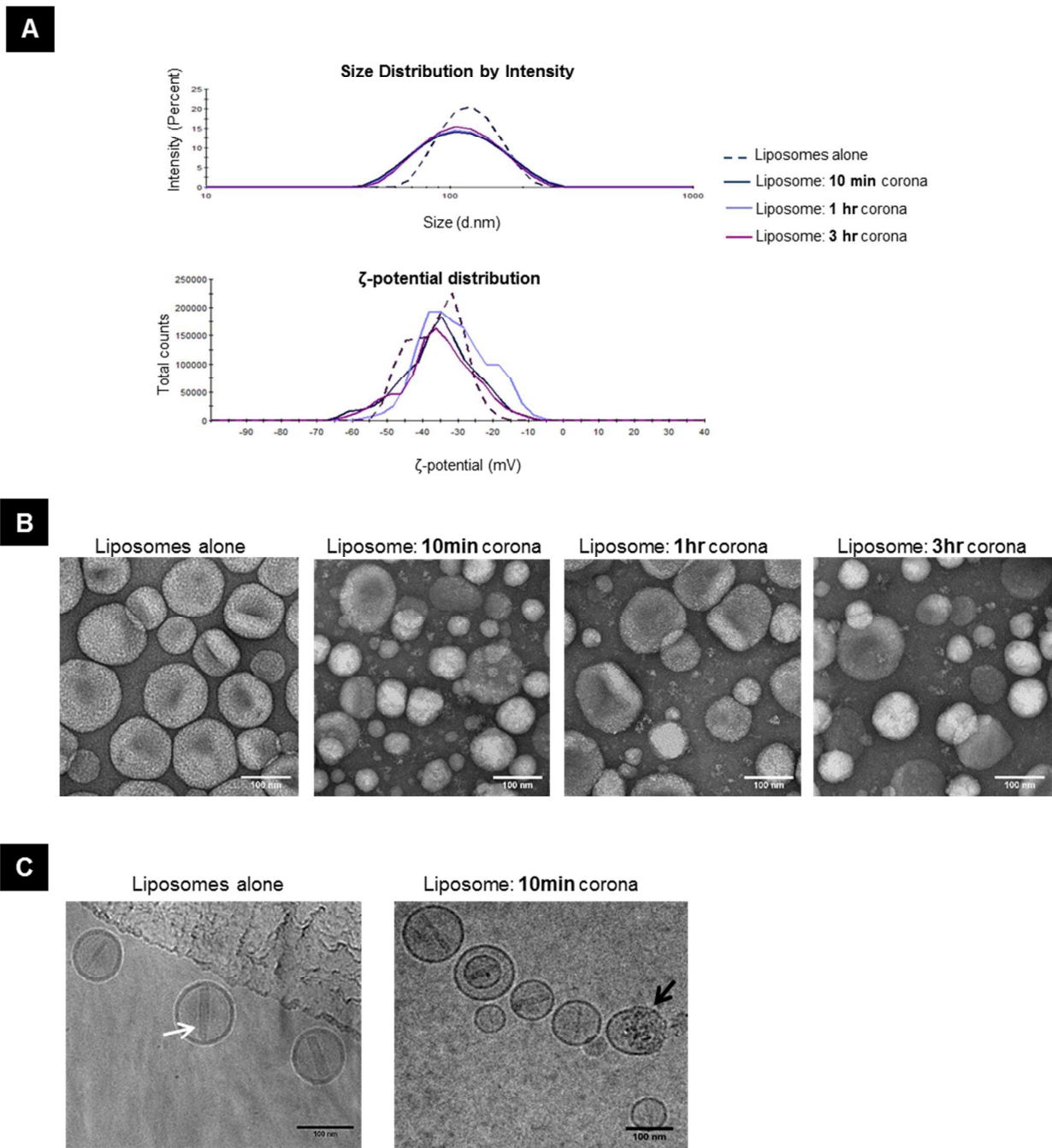


Figure 2

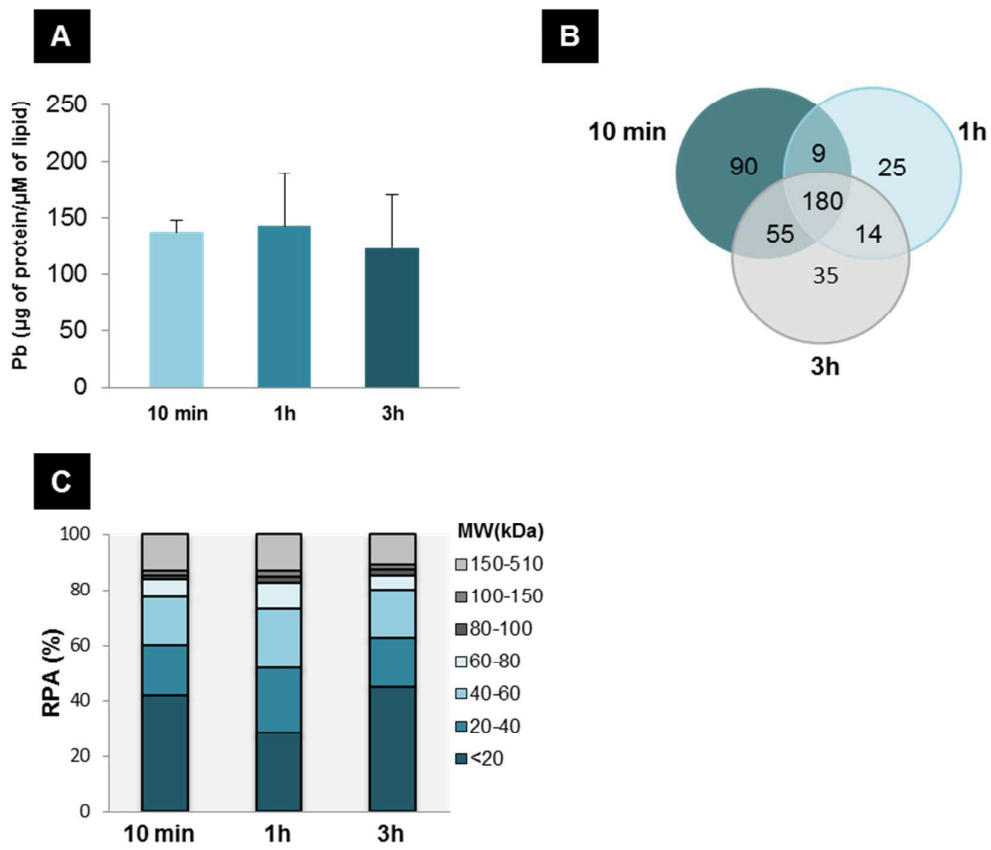
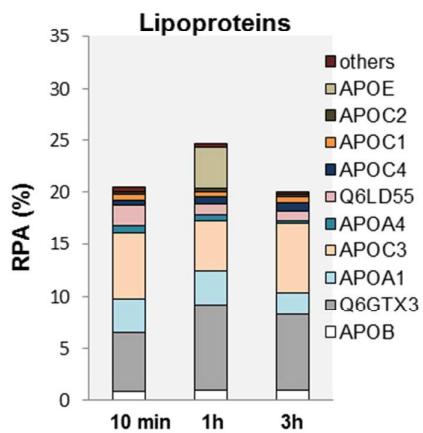


Figure 3

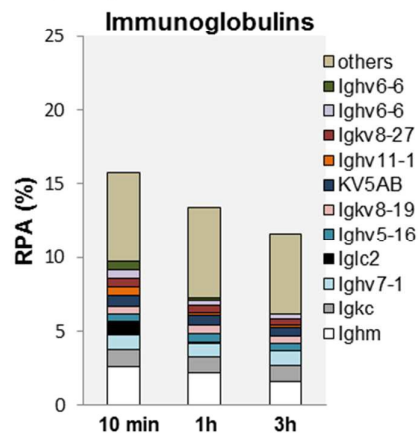
A

10 min		1 hr		3 hr	
Identified Protein	RPA	Identified Protein	RPA	Identified Protein	RPA
Alpha-2-macroglobulin	8.02 ± 1.45	Apolipoprotein E (PE=2 SV=1)	8.19 ± 1.71	Hemoglobin subunit beta-1	8.58 ± 1.93
Apolipoprotein C-III	6.37 ± 0.73	Alpha-2-macroglobulin	7.66 ± 1.06	Apolipoprotein E (PE=2 SV=1)	7.30 ± 0.27
Hemoglobin subunit beta-1	5.79 ± 0.13	Apolipoprotein C-III	4.86 ± 1.68	Apolipoprotein C-III	6.65 ± 0.69
Apolipoprotein E (PE=1 SV=2)	5.57 ± 0.33	Serum albumin	4.41 ± 1.74	Alpha-2-macroglobulin	6.42 ± 0.99
Beta-globin, Hbtt1 (A8DUK2)	4.48 ± 0.16	Apolipoprotein E (PE=1 SV=2)	3.87 ± 3.87	Beta-globin, Hbtt1 (A8DUK2)	6.02 ± 1.36
Apolipoprotein A-I	3.31 ± 0.27	Hemoglobin subunit beta-1	3.82 ± 0.16	Hemoglobin subunit beta-2	4.54 ± 1.09
Hemoglobin subunit beta-2	2.93 ± 0.13	Apolipoprotein A-I	3.25 ± 1.00	Alpha-globin	3.77 ± 0.89
Alpha-globin	2.74 ± 0.01	Serine protease inhibitor A3K	2.63 ± 0.93	Apolipoprotein A-I	2.14 ± 0.96
Ig mu chain C region	2.62 ± 0.21	Ig mu chain C region	2.23 ± 0.29	Fibrinogen beta chain	1.98 ± 0.61
Putative uncharacterized protein	2.54 ± 0.06	Hemoglobin subunit beta-2	2.20 ± 0.24	Fibrinogen gamma chain	1.92 ± 0.53
Serum albumin	2.35 ± 0.40	Alpha-globin	1.97 ± 0.53	Putative uncharacterized protein	1.68 ± 1.68
APOAII	1.89 ± 0.01	Serotransferrin	1.73 ± 0.64	Ig mu chain C region	1.56 ± 0.25
If kappa light chain (Fragment)	1.16 ± 0.11	Beta-globin, Hbtt1 (A8DUK2)	1.30 ± 1.30	Serum albumin	1.50 ± 0.59
Serine protease inhibitor A3K	1.14 ± 0.07	Complement C3	1.24 ± 0.43	Fibrinogen alpha chain	1.40 ± 0.53
Complement C3	0.95 ± 0.10	Aberrantly recombined kappa chain	1.10 ± 0.08	Serine protease inhibitor A3K	1.27 ± 0.50
Protein Ighv7-1	0.94 ± 0.11	Alpha-1B-glycoprotein	1.09 ± 0.34	If kappa light chain (Fragment)	1.18 ± 0.07
Serotransferrin	0.93 ± 0.08	APOAII	1.04 ± 0.31	APOAII	1.01 ± 0.05
Mannose-binding protein C	0.91 ± 0.03	If kappa light chain (Fragment)	1.02 ± 0.14	Protein Ighv7-1	0.96 ± 0.19
Apolipoprotein B-100	0.91 ± 0.06	Apolipoprotein B-100	0.97 ± 0.06	Protein Ighv1-18	0.94 ± 0.12
Ig lambda-2 chain C region	0.90 ± 0.76	Protein Ighv7-1	0.95 ± 0.18	Apolipoprotein B-100	0.92 ± 0.10
Anti-colorectal carcinoma light chain	0.86 ± 0.43	Alpha-1-antitrypsin 1-3	0.94 ± 0.26	Anti-colorectal carcinoma light chain	0.85 ± 0.43

B



C



D

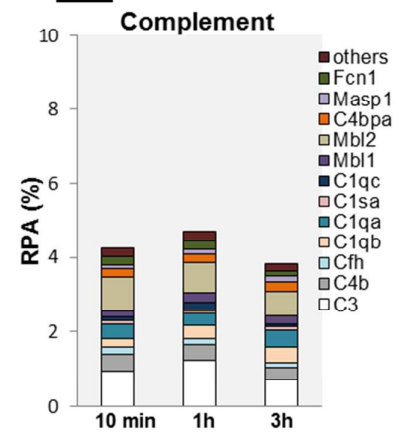


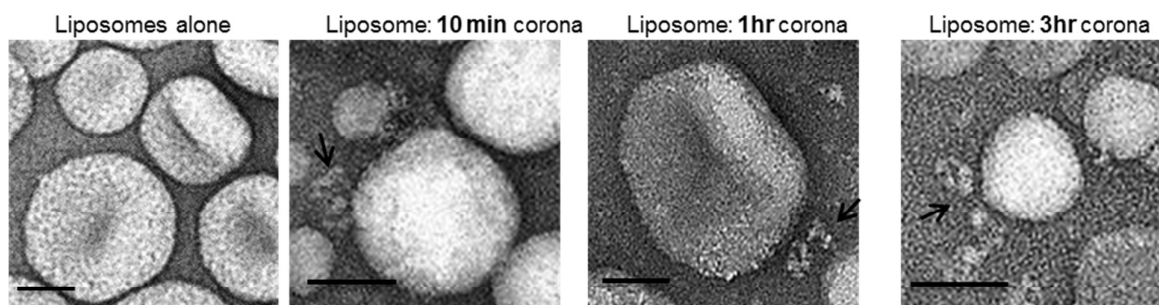
Figure 4

Supporting Table

Table S1: The physicochemical characteristics of PEGylated liposomal doxorubicin before and after extraction from blood circulation. Mean vesicle diameter (nm) and ζ -potential (mV) data from DLS and surface charge electrophoresis are shown.

Liposome type	Size (nm)	ζ -potential (mV)	PDI
Liposomes alone (HSPC:CHOL:DSPE-PEG2000) (56.3:38.2:5.5)	114.6 \pm 1.752	-36.2 \pm 0.85	0.056 \pm 0.018
Liposome: 10min corona	102.0 \pm 3.107	-35.5 \pm 1.20	0.123 \pm 0.012
Liposome: 1hr corona	104.0 \pm 1.662	-33.5 \pm 3.16	0.127 \pm 0.032
Liposome: 3hr corona	103.1 \pm 4.152	-34.1 \pm 2.37	0.104 \pm 0.015

Supporting Figures



FigureS1: Negative stain TEM imaging of liposomes before their interaction with plasma proteins and **10 min**, **1h** and **3h** after their i.v. injection and recovery from CD-1 mice. Arrows show the presence of proteins around the surface of liposomes. All scale bars are 50nm.

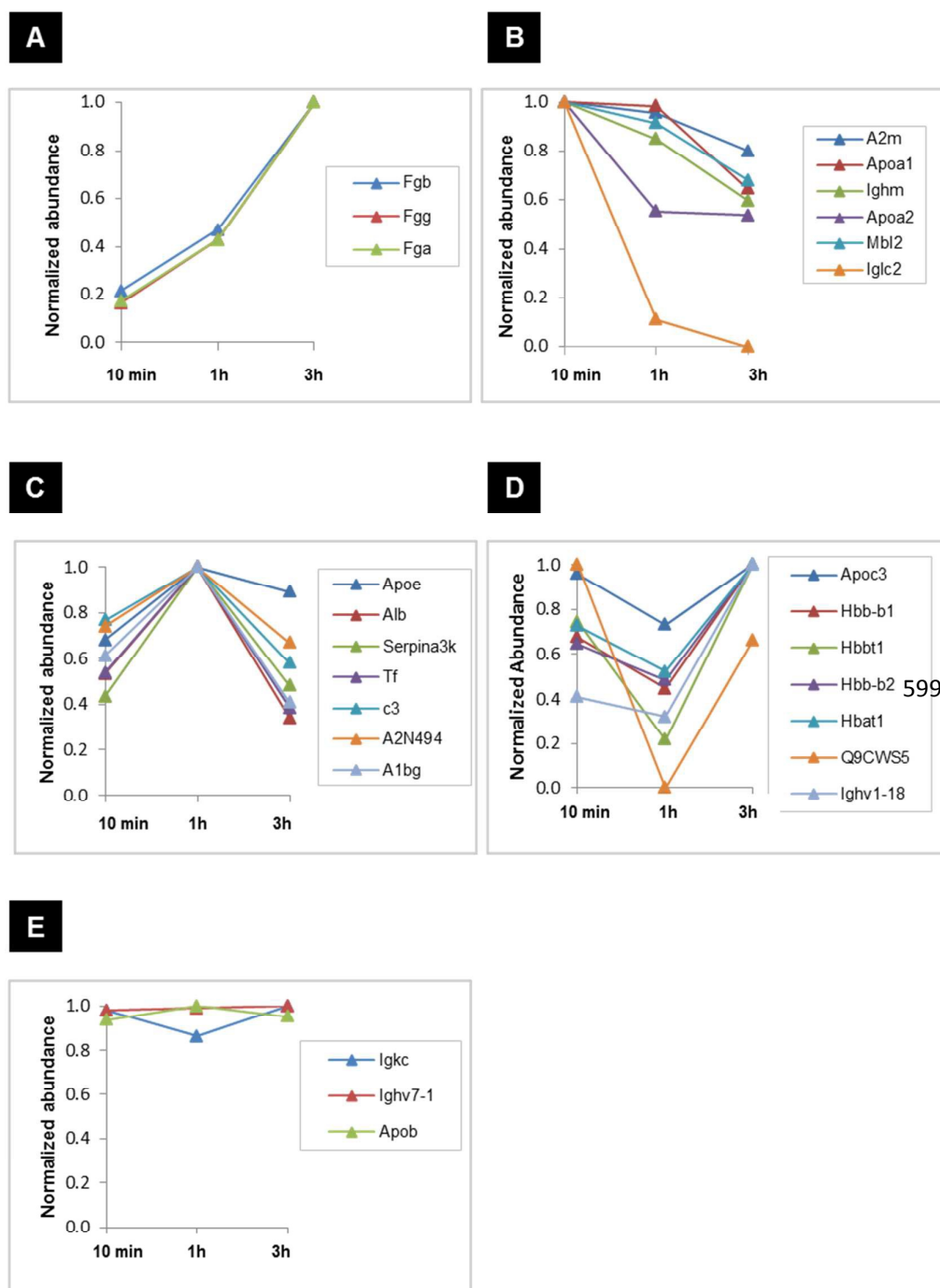


Figure S2: Protein binding kinetics during corona evolution. Relative values were normalized to the maximum amount (set to 1) across the three time points for each of the top-20 proteins. Corona proteins were classified into five groups: **(A)** Proteins displaying increased binding over time; **(B)** Proteins displaying reduced binding over time; **(C)** Proteins characterized by low abundance at the early ($t=10\text{min}$) and late time points ($t=3\text{h}$) and higher abundance at intermediate time point ($t=1\text{h}$); **(D)** Proteins characterized by high abundance at the early ($t=10\text{min}$) and late time points ($t=3\text{h}$) and lower abundance at intermediate time point ($t=1\text{h}$); **(E)** Proteins with constant abundance over time.